minerals

MDPI

Article

Rapid Removal of Cr(VI) from Aqueous Solution Using Polycationic/Di-Metallic Adsorbent Synthesized Using Fe^{3+}/Al^{3+} Recovered from Real Acid Mine Drainage

Khathutshelo Lilith Muedi [1], Vhahangwele Masindi [2,3], Johannes Philippus Maree [4] and Hendrik Gideon Brink [1,*]

[1] Department of Chemical Engineering, Faculty of Engineering, Built Environment and Information Technology, University of Pretoria, Pretoria 0028, South Africa
[2] Magalies Water, Scientific Services, Research & Development Division, Erf 3475, Stoffberg Street, Brits 0250, South Africa
[3] Department of Environmental Sciences, School of Agriculture and Environmental Sciences, University of South Africa (UNISA), P.O. Box 392, Florida 1710, South Africa
[4] Department of Water and Sanitation, University of Limpopo, University Street, Polokwane 0727, South Africa
* Correspondence: deon.brink@up.ac.za; Tel.: +27-84-206-8338

Abstract: The mining of valuable minerals from wastewater streams is attractive as it promotes a circular economy, wastewater beneficiation, and valorisation. To this end, the current study evaluated the rapid removal of aqueous Cr(VI) by polycationic/di-metallic Fe/Al (PDFe/Al) adsorbent recovered from real acid mine drainage (AMD). Optimal conditions for Cr(VI) removal were 50 mg/L initial Cr(VI), 3 g PDFe/Al, initial pH = 3, 180 min equilibration time and temperature = 45 °C. Optimal conditions resulted in ≥95% removal of Cr(VI), and a maximum adsorption capacity of Q = 6.90 mg/g. Adsorption kinetics followed a two-phase pseudo-first-order behaviour, i.e., a fast initial Cr(VI) removal (likely due to fast initial adsorption) followed by a slower secondary Cr(VI) removal (likely from Cr(VI) to Cr(III) reduction on the surface). More than 90% of adsorbed Cr(VI) could be recovered after five adsorption–desorption cycles. A reaction mechanism involving a rapid adsorption onto at least two distinct surfaces followed by slower in situ Cr(VI) reduction, as well as adsorption-induced internal surface strains and consequent internal surface area magnification, was proposed. This study demonstrated a rapid, effective, and economical application of PDFe/Al recovered from *bona fide* AMD to treat Cr(VI)-contaminated wastewater.

Keywords: chromium removal; acid mine drainage; wastewater streams; circular economy; wastewater beneficiation; polycationic/di-metallic adsorbent (nanocomposite)

Citation: Muedi, K.L.; Masindi, V.; Maree, J.P.; Brink, H.G. Rapid Removal of Cr(VI) from Aqueous Solution Using Polycationic/Di-Metallic Adsorbent Synthesized Using Fe^{3+}/Al^{3+} Recovered from Real Acid Mine Drainage. *Minerals* **2022**, *12*, 1318. https://doi.org/10.3390/min12101318

Academic Editor: María Ángeles Martín-Lara

Received: 13 September 2022
Accepted: 13 October 2022
Published: 19 October 2022

1. Introduction

Despite the socio-economic benefits provided by the gold and coal industries, the mining of these commodities is notorious for inducing significant environmental degradation [1,2]. Mining entails the excavation of large quantities of rock to obtain the targeted minerals or minerals. During the extraction of mineral resources, hard rock (such as gold) or soft rock (such as coal) is exposed to air which typically leads to the oxidation of associated minerals. Generally, coal and gold are associated with sulphide-bearing minerals, e.g., FeS, FeAsS, ZnS, CuS, and NiS amongst others, resulting in the production of metalliferous acidic drainage rich in sulphates [3,4]. Due to the acidic nature of this wastewater stream, minerals in the surrounding geology leach into the surrounding body of water hence increasing the electrical conductivity and total dissolved solids. Acid mine drainage (AMD) or acid rock drainage (ARD) generally contains significant quantities of Al, Fe, Mn, and sulphate as major contaminants. However, the presence of minor, but not insignificant, levels of toxic and hazardous heavy metals, radionuclides, metalloids, oxyanions, and rare

earth metals has been reported [4–8]. As such, the AMD matrix needs to be contained and treated prior to discharge to the receiving environments [9,10].

Research by the authors of the study demonstrated the valorisation of acid mine drainage for the recovery of Al/Fe tri-valent metals through the synthesis of an adsorbent that was tested for the removal of arsenic [1] and Congo Red [2] from wastewater. The synthesized adsorbent achieved remarkably high adsorption capacities for both As (102–129 $mg \cdot g^{-1}$) and Congo Red (411 $mg \cdot g^{-1}$), illustrating the potential of the recovered adsorbent for the effective treatment of hazardous pollutants from solution.

Chromium is used as an additive in myriad production processes; chromium is a crucial component of chemical production, metallurgical industries, refractories, and foundries [11]. A report by the US Geological Survey indicated that South Africa and Kazakhstan are the world's largest producers of chromium, with approximately 95 percent of global chromium reserves [12]. This toxic and hazardous chemical species emanates from natural (geogenic) and man-made (anthropogenic) sources. Natural sources include rocks, volcanic eruptions, and minerals, while anthropogenic sources comprise mining, tanning, and manufacturing of paints, plastics, ceramics, glass, salts, dyes, and dietary supplements. These sources release chromium rich effluents to different spheres of the environment [13–15].

(Eco)-toxicological studies highlighted that the intake of water with elevated levels of chromium ions, specifically the hexavalent chromium, could lead to direct detrimental impacts on human health through bioaccumulation, animals, aquatic organisms, and the environment at large [16]. According to toxicological study, the maximum allowed limit in drinking water should be $\leq$0.05 ppm [17]. In response to this stringent regulatory framework and standard, various studies devised ways to treat, remove, and recover chromium ions from the water and wastewater matrices. These include electrocoagulation [18], nanofiltration [19], freeze desalination [20], ion exchange [21], photo-catalysis [22], adsorption, precipitation, bio-(phyto)-remediation, and crystallization [11,13,14,23–25]. However, these technologies still pose challenges regarding operational cost and disposal of secondary sludge which reduces their desirability. Consequently, adsorption has emerged as a promising technology due to its effectiveness, affordable costs, and reliance on locally available materials [1,9]. However, the dependence of traditional adsorbent manufacturing on virgin and pristine materials poses notable risks to the environment; hence, there is a demand to find alternative sources of materials to produce adsorbents.

The use of Fe and Al adsorbents has been demonstrated successfully for the treatment of aqueous Cr(VI) [26–30], and dominant mechanisms reported involved ion exchange [26,27,30], surface reduction of Cr(VI) to Cr(III) reduction [28], and electrostatic forces [29,30].

The current study will be the first known to explore the feasibility of using Polycationic/dimetal Al^{3+} and Fe^{3+}-derived adsorbent (PDFe/Al) synthesized using real AMD for the removal of hexavalent chromium from aqueous solution. Chiefly, wastewater treatment technologies need to be feasible, effective, and affordable. Therefore, this study introduces an affordable and effective technique to treat chromium-contaminated water using a material recovered from acid mine drainage—a well-known environmental hazard—thereby providing a potential solution for both waste streams.

2. Materials and Methods

2.1. Sample Collection and Preparation of Working Solution

Crude acid mine effluent (AMD) was collected from a coal mine in Mpumalanga, South Africa. Potassium dichromate ($K_2Cr_2O_7$) was purchased from Sigma Aldrich. Caustic soda (NaOH), sulfuric acid (98.5% H_2SO_4) and hydrochloric acid (37% HCl) were purchased from Merck. All chemicals were used as received, with no further purification. Ultrapure water (18.2 MΩ-cm) was used for the synthesis of all solutions. For the preparation of hexavalent chromium (Cr(VI)) stock solution, $K_2Cr_2O_7$ salt was used. To avoid contamination, experimental glassware was meticulously cleaned before and after each use. To simulate the working solution, 1000 $mg \cdot L^{-1}$ Cr(VI) stock solution was prepared by dissolving 2.835 g of

$K_2Cr_2O_7$ salt in ultrapure water (18.2 MΩ-cm) in a 1000 mL volumetric flask. The container was then filled to the specified level (mark). Thereafter, serial dilutions were made from the prepared working solution.

2.2. Synthesis of PDFe/Al from Authentic AMD

The PDFe/Al was synthesized using the method previous described [1,2]. A known AMD volume was reacted with 30% NaOH at a pH = 4.5 to selectively precipitate trivalent Fe and Al as -OOH compounds and the mixture was stirred for 30 min at room temperature with an overhead stirrer. Subsequently, the mixture was heated to 100 °C while stirring. The precipitates were vacuum filtered (Whatman® Grade 40 ash-less) and dried. The recovered material was vibratory-ball-milled at 700 rpm and calcined at 800 °C. The milled samples were sieved to a maximum size of 32 µm and stored in a plastic "zip-lock" bag until use.

2.3. Optimisation Studies

The synthesised Fe/Al di-metal composite was then used for the removal of Cr(VI) from aqueous solutions. Optimised parameters include initial Cr(VI) concentration (mg/L), adsorbent dose (g), agitation time (g), temperature (°C), and initial solution pH. In all experiments, 250 mL of Cr(VI) rich solutions was added to 500 mL volumetric flasks. All experiments were performed in triplicate for quality control and quality assurance, and the data were reported as mean ± standard deviations. The impacts of various parameters on the adsorption process were investigated, and the results are summarized in Table 1.

Table 1. Parameters tested for Cr(VI) adsorption using PDFe/Al.

Experiment No	Initial Cr(VI) Concentration (mg/L)	Initial pH	Adsorbent Dose (g)	Agitation Time (min)	Temperature (°C)
1	1; 5; 10; 20; 30; 40; 50; 100; 150; 200	4–5	1	180	25
2	10	2, 3, 4, 5, 6, 7, 8, 9, 10 (±0.2)	1	180	25
3	10	4–5	0.1; 0.5; 1; 2; 3; 4; 5 (±0.0005)	180	25
4	10	4–5	1	10; 30; 60; 90; 120; 180; 240; 300	25
5	10	4–5	1	180	25; 35; 45; 55; 65

The various initial concentration were obtained by diluting a concentrated stock solution of 1000 mg·L^{-1} Cr(VI) as shown in Table 1. The effect of agitation time was determined by measuring the Cr(VI) concentrations at various time. The influence of initial solution pH was investigated by changing the pH with 0.1 M NaOH/0.1 HNO_3. Batch adsorption studies were carried out in a thermal shaker/incubator at various temperatures.

2.4. Characterisation of the Feedstock and Product Minerals

Inductively Coupled Plasma Mass Spectrometry (ICP-MS) was used to assess the fate of Cr(VI) in aqueous samples (7500ce, Agilent, Alpharetta, GA, USA).

The PDFe/Al and Cr-residue products were analysed as described previously [1,2] using X-ray diffraction (XRD: Panalytical X'PertPRO (Malvern Panalytical, Malvern, UK) equipped with a Cu-K radiation source), Htable igh-resolution scanning electron micrographs (HR-SEM-EDX) were used to examine the surface morphology and composition of solid materials (CarlZeiss Sigma VP FE-SEM with Oxford EDX Sputtering System, Carl Zeiss AG, Oberkochen, Germany). Fourier Transform Infrared Spectrometer—Attenuated Total Reflectance (FTIR-ATR: Perkin-Elmer Spectrum 100), BET (Micromeritics Tri-Star II 3020, Surface area and porosity, Poretech CC, Jefferson, TX, USA), and Thermo Gravimetric Analyzer (TGA: SelectScience TGA Q500, TA instruments, Bath, UK).

2.5. Point of Zero Charge (PZC)

The point of zero charge (PZC) of the PDFe/Al was determined using a method proposed by Smičiklas et al. (2000) [31]. 0.1 g of the PDFe/Al were added to each of nine flasks containing 50 mL 0.1 M KNO_3 solutions adjusted to pH 2–10 (using 0.1 M HNO_3 and/or NaOH) and left to equilibrate for 24 h at ± 25 °C. Subsequently, the suspensions were filtered, and the pH of the filtrates determined.

2.6. PDFe/Al Adsorption Capacity and Removal Efficiency

2.6.1. Adsorption Capacity

The adsorption capacities of PDFe/Al were determined using Equation (1) [32]:

$$Q = \frac{(C_0 - C) \times V}{m} \quad (1)$$

where Q (mg·g^{-1}) is the adsorption capacity; C_0 (mg·L^{-1}) is the initial concentration of Cr(VI), C (mg·L^{-1}) is the measured concentration of Cr(VI), respectively; V (L) is the volume of the Cr(VI) solution; and m (g) is the dosage of PDFe/Al.

2.6.2. Percentage Removal

The removal efficiency of Cr(VI) by PDFe/Al was determined using Equation (2):

$$\%R_e = \frac{C_0 - C_e}{C_0} \times 100 \quad (2)$$

where $\%R_e$ is the removal efficiency of the PDFe/Al; C_0 is the initial Cr(VI) concentration (mg/L); C_e is the equilibrium Cr(VI) concentration (mg·L^{-1}).

2.7. Regeneration Study

Kumari et al. (2006) [32] described a method for studying the regeneration of PDFe/Als. 250 mL of a 150 mg·L^{-1} Cr(VI) solution was treated with 1 g of PDFe/Al for 90 min in a batch experiment. The adsobent was centrifuged to separate it from the supernatant and the recovered and washed five times with 250 mL ultra-pure water (to remove residual Cr(VI)) and dried. 250 mL of 0.1 M HNO_3 was added to the dried sample at room temperature, the HNO_3 extract was collected and tested for Cr(VI) ions. Equation (3) was used to calculate the regeneration percentage:

$$\%\text{Desorption} = \frac{C_{des}}{C_o} \times 100 \quad (3)$$

where C_{des} (mg·L^{-1}) is the concentration of Cr(VI) ions in the desorption eluent; C_o (mg·L^{-1}) is the initial concentration of Cr(VI) ions.

3. Results

3.1. Characterisation of PDFe/Al before and after Cr(VI) Adsorption

3.1.1. FTIR Analysis

Figure 1 depicts the functional groups of the PDFe/Al before and after Cr(VI) adsorption using a Fourier Transform Infrared Spectrometer (FTIR). Table 2 summarises the peak positions for raw PDFe/Al and Cr-PDFe/Al. For the raw PDFe/Al and Cr- PDFe/Al, significant -OH stretching was measured between 4000 and 3500 cm^{-1}. At *circa* 1630 cm^{-1} and 1100 cm^{-1}, HOH stretching is observed [33]. After Cr(VI) adsorption, a change in the stretching of HOH group is observed as a shift of wave band 1096.3 to 1103.2 cm^{-1} [34]. The characteristic peaks for aluminium oxides at ~535 cm^{-1} [35] ~606 cm^{-1} and ~705 cm^{-1} [36], and iron oxides at ~606 cm^{-1} and ~795 cm^{-1} [36,37] provide evidence for the successful synthesis of Fe/Al oxides. In addition, a new absorption band at, corresponding to O-Cr-O,

is observed at 610.9 cm^{-1} [38,39], confirming the successful adsorption of Cr(VI) to the adsorbent surface.

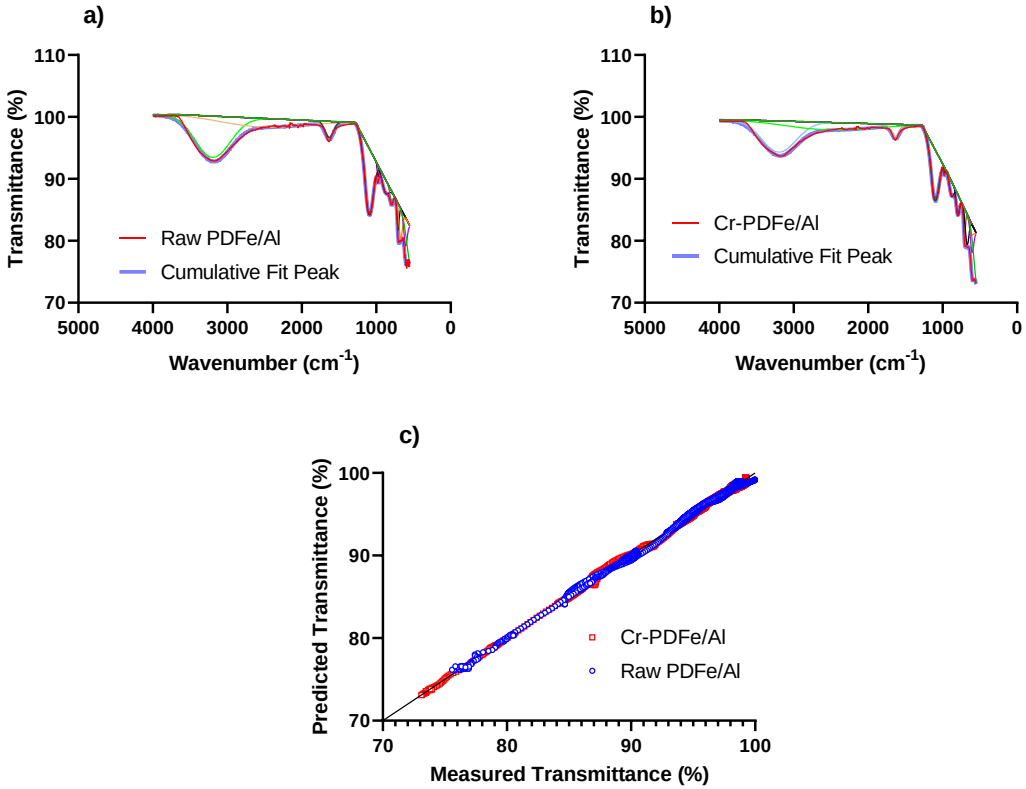

Figure 1. The deconvoluted peaks of the FTIR spectra for PDFe/Al (**a**) before and (**b**) after Cr(VI) adsorption. (**c**) shows the Transmittance for Raw PDFe/Al and Cr-PDFe/Al.

Table 2. A summary of peak positions for raw PDFe/Al and Cr-PDFe/Al.

Raw PDFe/Al	Cr-PDFe/Al	Likely Attributable Source
535.5	532.8	AlOOH [35], Si-O-Al [28]
606.4	604.4	Fe-O [36,37], O-Al-O [36]
-	610.9	O-Cr-O [38,39]
705.2	704.9	AlOOH [36]
795.3	796.2	Fe-O [36], Silica [28]
976.4	976.9	Si-O [40]
1096.3	1103.2	HOH stretching [33], S-O groups [41], Si-O-Al linkages [40]
1629.9	1630.2	HOH stretching [28,33]
3197.3	3200.0	O-H [1,2]

3.1.2. XRD Mineralogical Composition

Figure 2 depicts the XRD analyses of the PDFe/Al before and after Cr(VI) adsorption. Iron (Fe) is observed to be the dominant species in the PDFe/Al in the form of goethite/iron(III) oxide hydroxide (FeO(OH)) with clear diffraction peaks showing the crystallinity of the adsorbent and some amorphousness. In addition, the presence of aluminium in the form of aluminium oxide (Al_2O_3) is observed, thus confirming the composite nature of the material.

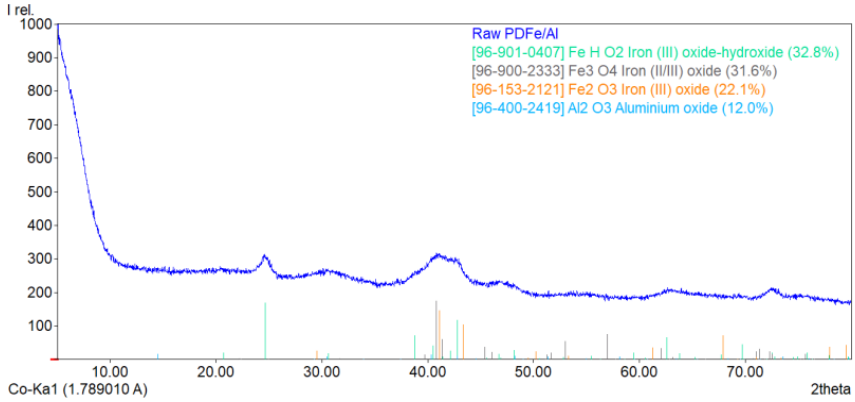

Figure 2. XRD diffractogram of the PDFe/Al before Cr(VI) adsorption. Error between selected phases and experimental profile = 3.3%.

Significant peaks between 2θ ≈ 35° to 50° are observed to have increased after Cr(VI) adsorption. This is attributed to the diffusion of Cr(VI) ions into the pores of the PDFe/Al adsorbent through chemisorption, with the subsequent reduction to Cr(III) (as confirmed by the presence of CrOOH) [42].

Figure 3 shows the diffractogram of the PDFe/Al after Cr(VI) adsorption.

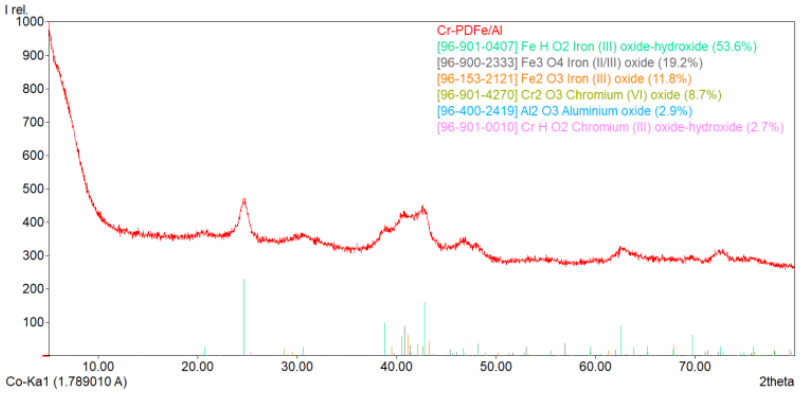

Figure 3. XRD diffractogram of the PDFe/Al after Cr(VI) adsorption. Error between selected phases and experimental profile = 3.4%.

Table 3 shows the EDS and XRF mole percentage results for raw PDFe/Al and Cr-PDFe/Al. Characterisation before Cr(VI) adsorption shows the presence of Fe and Al in the synthesised adsorbent which confirm the dimetallic nature of the material.

The presence of Fe and S shows that AMD was generated from pyrite oxidation. The presence of Si, Ca, Mg, and other trace elements in the material are impurities that resulted from co-precipitation from AMD. After Cr(VI) adsorption, it is observed that chromium is the only element showing a significant difference between the PDFe/Al and Cr-PDFe/Al. Overall, the composition of Fe, Al, O and C was observed to be preserved during adsorption, therefore demonstrating the chemically stability of the material.

Figure 4 shows the relationship between 2θ values for PDFe/Al before and after Cr(VI) adsorption.

As indicated in Figure 4, the plot for 2θ values for PDFe/Al before and after Cr(VI) adsorption shows a clear shift in 2θ values of 0.66° thus confirming internal adsorption induced strains as previously reported in Muedi et al. 2022 [2].

3.1.3. BET Surface and Porosity Analysis

Figure 5 and Table 4 depicts the porosity of the PDFe/Al before and after Cr(VI) adsorption using Brunauer-Emmet-Teller (BET). It is clear that a significant increase in

both the internal surface area and volume was observed The total surface area of the raw PDFe/Al was reported to be around 37.5841 m^2/g, which then changed to 95.5269 m^2/g after Cr(VI) adsorption, while an eight-fold increase in internal pore volume (0.003 cm^3/g to 0.02 cm^3/g) was observed after Cr(VI) adsorption. These results are consistent with that observed previously for Congo Red adsorption [2].

Table 3. EDS and XRF mole percentage results.

	PDFe/Al			Cr-PDFe/Al			Fe/Al vs. Cr-PDFe/Al
Element	**EDS**	**XRF**	***p*-Value [1]**	**EDS**	**XRF**	***p*-Value [2]**	***p*-Value [3]**
Fe	21.11 ± 10.42	37.51	0.22	32.38 ± 15.39	38.91	0.72	0.21
O	67.99 ± 2.53	59.83	0.042	59.75 ± 19.51	60.07	0.99	0.38
S	7.34 ± 3.72	0.24	0.16	4.59 ± 2.52	0.07	0.18	0.21
Cr [4]	0 ± 0	0.00	-	1.46 ± 0.57	0.08	0.091	0.00043
Al	0.83 ± 0.38	1.15	0.49	1.02 ± 0.47	0.62	0.48	0.51
Si	0.19 ± 0.32	0.14	0.90	0.07 ± 0.11	0.13	0.65	0.46
K	0 ± 0	0.00	-	0.15 ± 0.1	0.00	0.24	0.01
Ca	1.75 ± 3.74	0.15	0.72	0 ± 0	0.00	-	0.33
Cl	0.51 ± 1.13	0.00	0.70	0 ± 0	0.00	-	0.35
Na	0.18 ± 0.4	0.62	0.37	0.3 ± 0.31	0.00	0.43	0.61
Mg	0.11 ± 0.25	0.29	0.56	0.2 ± 0.32	0.00	0.59	0.63
Ti	0 ± 0	0.00	0.22	0.06 ± 0.13	0.00	0.70	0.35
Total	100.00 ± 0.00	99.94	-	100.00 ± 0.00	99.89	-	-

[1] *p*-value for two tailed *t*-test comparison between EDS and XRF for PDFe/Al; [2] *p*-value for two tailed *t*-test comparison between EDS and XRF for Cr-PDFe/Al; [3] *p*-value for two-tailed *t*-test comparison between EDS data sets for PDFe/Al and Cr-PDFe/Al (5 repeat measurements each); [4] Only element showing a significant difference between the PDFe/Al and Cr-PDFe/Al when considering the adjusted *p*-value significance level as calculated using the Holm-Šídák method.

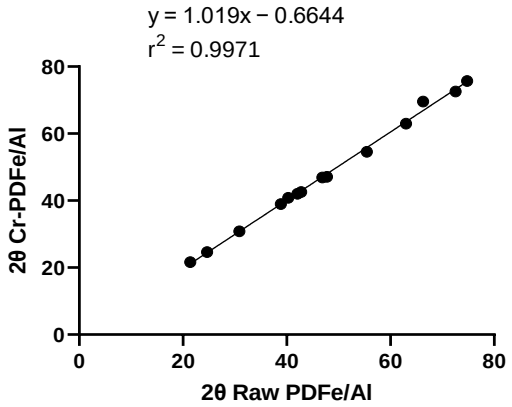

Figure 4. 2θ values for PDFe/Al before and after Cr(VI) adsorption.

The increased total surface area implies that the adsorbed chemical has the potential to enhance the adsorbent's surface area, indicating the material's potential for subsequent usage after Cr(VI) ion adsorption.

Figure 6 depicts the nitrogen adsorption–desorption isotherms of the produced PDFe/Al before and after Cr(VI) adsorption. The adsorbed quantities increased as relative pressure increased, which could indicate that the adsorbent's non-rigid nature and the placement of the distinctive shoulder are compatible with condensate destabilization at the P/P0 ratio, which is limiting the entire process. Furthermore, type IV adsorption isotherm behaviour was observed for both the raw PDFe/Al and the Cr-adsorbed PDFe/Al.

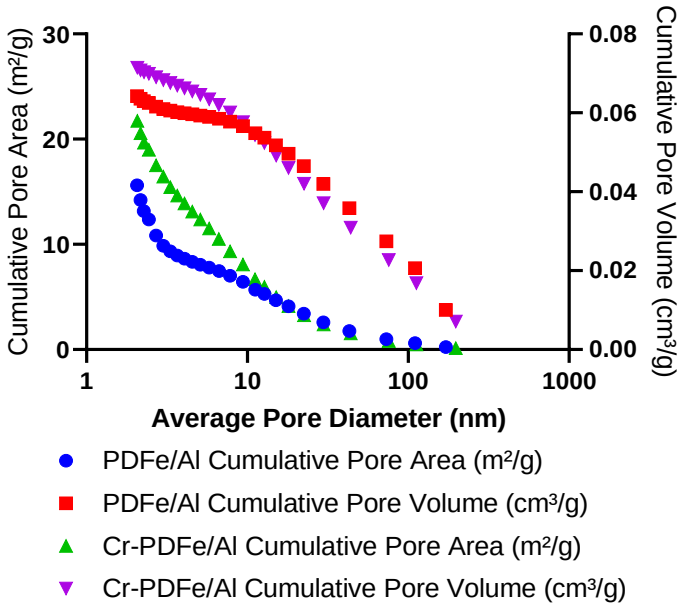

Figure 5. Porosity of the PDFe/Al before and after Cr(VI) adsorption.

Table 4. Shows a summary of the porosity of PDFe/Al before and after Cr(VI) adsorption.

Material	Parameter	Value
PDFe/Al	Total Surface Area (BET):	37.5841 m^2/g
	Micropore Volume:	0.003066 cm^3/g
	Micropore Area:	13.6686 m^2/g
	External Surface Area:	23.9156 m^2/g
Cr-PDFe/Al	Total Surface Area (BET):	95.5269 m^2/g
	Micropore Volume:	0.020797 cm^3/g
	Micropore Area:	52.9926 m^2/g
	External Surface Area:	42.5343 m^2/g

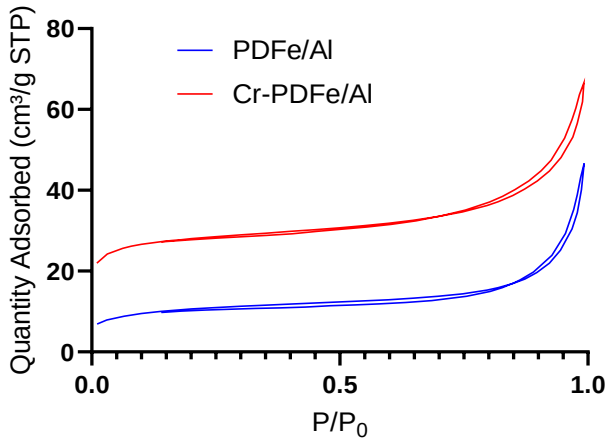

Figure 6. The nitrogen adsorption–desorption isotherms of the synthesized PDFe/Al before and after Cr(VI) adsorption.

3.1.4. SEM Morphology

Figure 7 shows the morphology of the PDFe/Al before and after Cr(VI) adsorption using scanning electron microscopy (SEM).

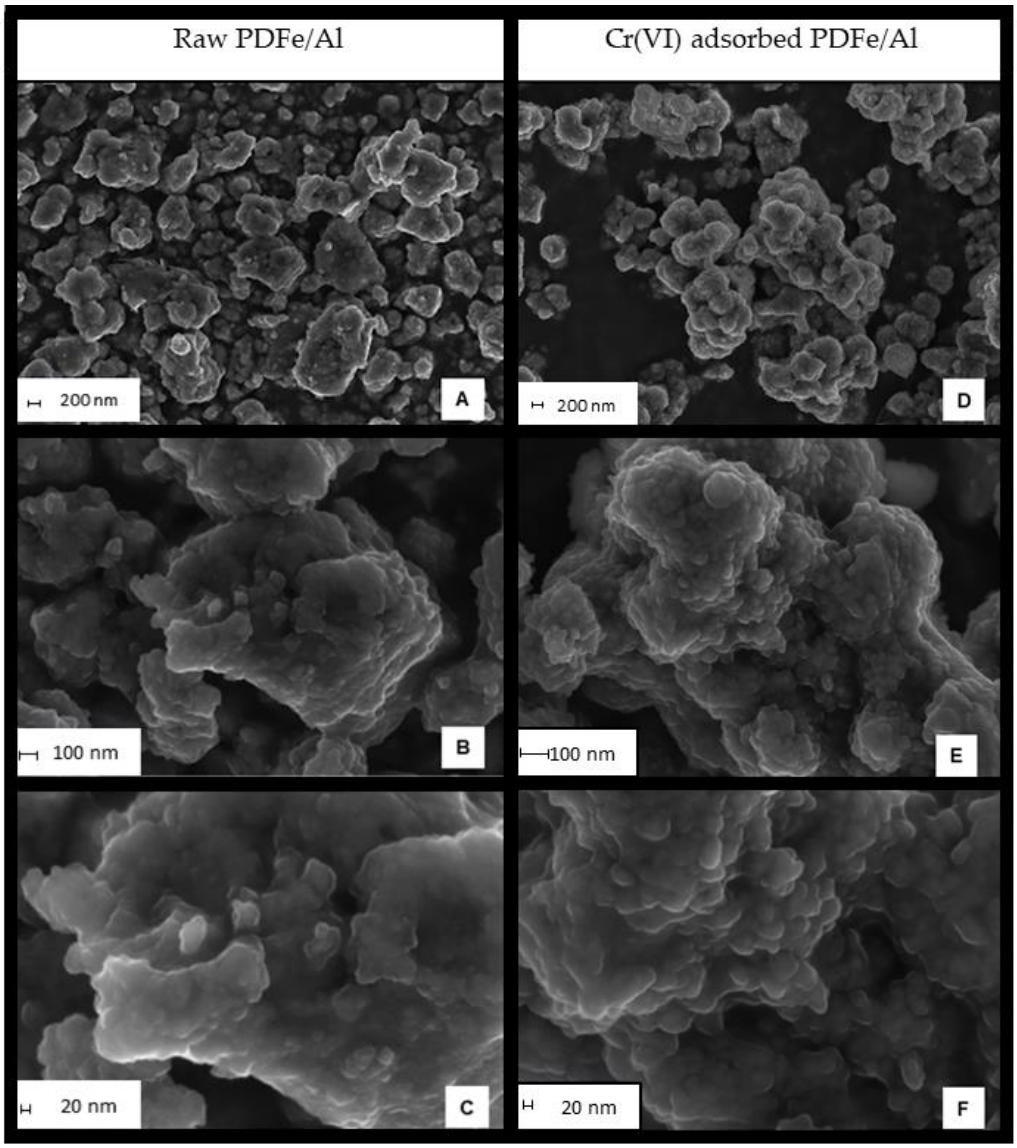

Figure 7. Morphology of the PDFe/Al before adsorption (**A**–**C**) and after Cr(VI) (**D**–**F**) adsorption.

The morphological features of the synthesized PDFe/Al before and after Cr(VI) adsorption are presented in Figure 7. Figure 7A–C show the morphology of raw PDFe/Als of various sizes, with non-uniform pressed-like structures with irregular agglomerates scattered unevenly. Figure 7D–F show the morphology of PDFe/Als following Cr(VI) adsorption in various sizes, with blood cell-like formations that are irregularly dispersed and lumped together. The shift in structural forms could indicate the presence of chromium heavy metal in the material.

3.1.5. EDX Elemental Mapping

Figure 8 shows the mapping of the elemental composition of the PDFe/Al before and after Cr(VI) adsorption using energy dispersive X-ray (EDX). The raw PDFe/Al confirms the co-precipitation of Fe and Al from AMD, (Figure 8A–D). Figure 8E–H illustrates the elemental composition of the material after Cr(VI) adsorption, where chromium is observed to be present.

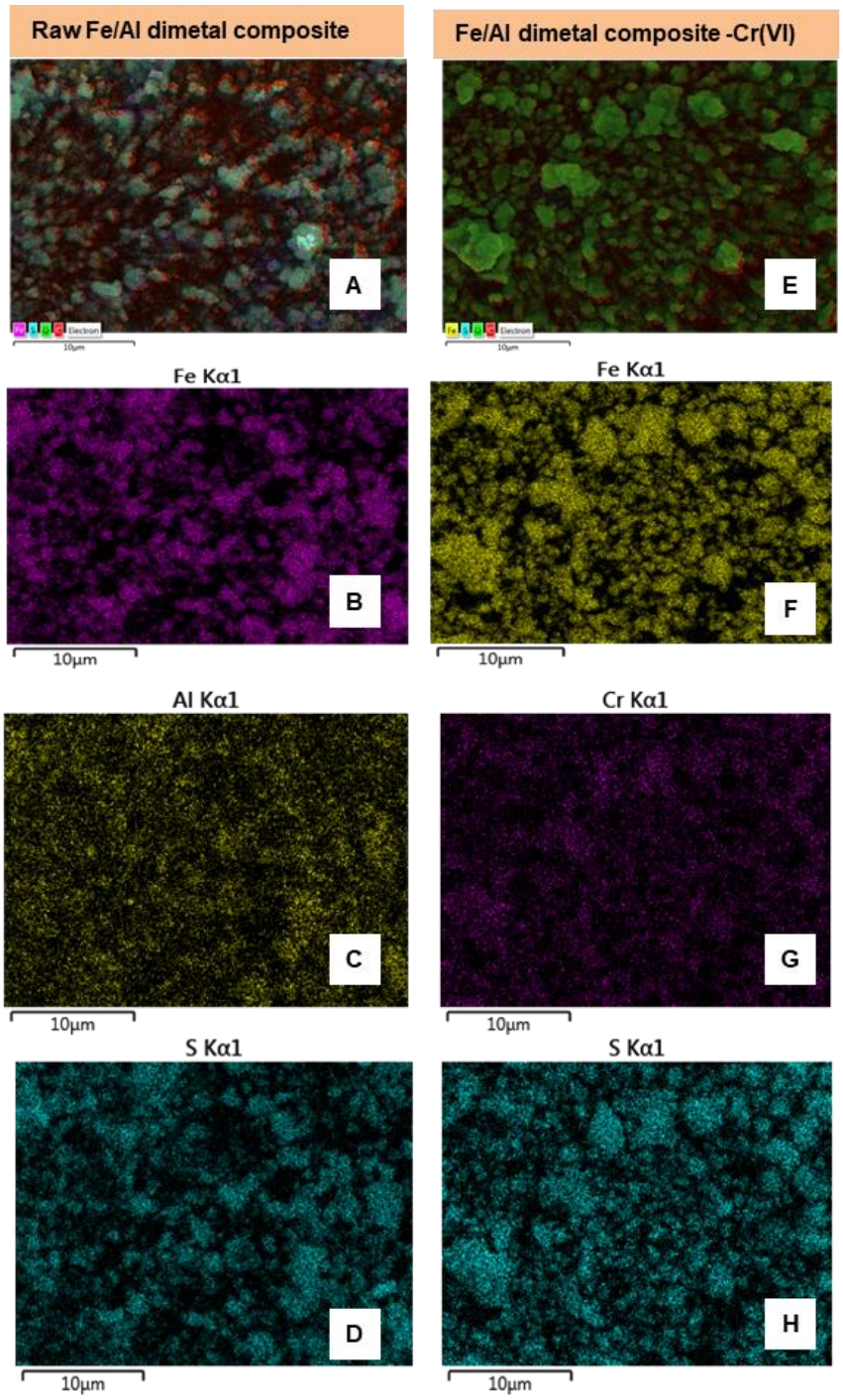

Figure 8. Mapping of elemental composition of the PDFe/Al before adsorption (**A**–**D**) and after Cr(VI) (**E**–**H**) adsorption.

3.1.6. TGA Thermal Stability

The thermal stability of PDFe/Al before and after Cr(VI) adsorption is demonstrated in Figure 9. The calcination process was broken down into three stages, with the first involving the loss of moisture from the material at temperatures ranging from 100 to 350 °C. At temperatures between 400 and 550 °C, the second step involves the loss of chemically bonded HOH, while the third stage involves the loss of the hydroxyl group (-OH) at temperatures over 550 °C.

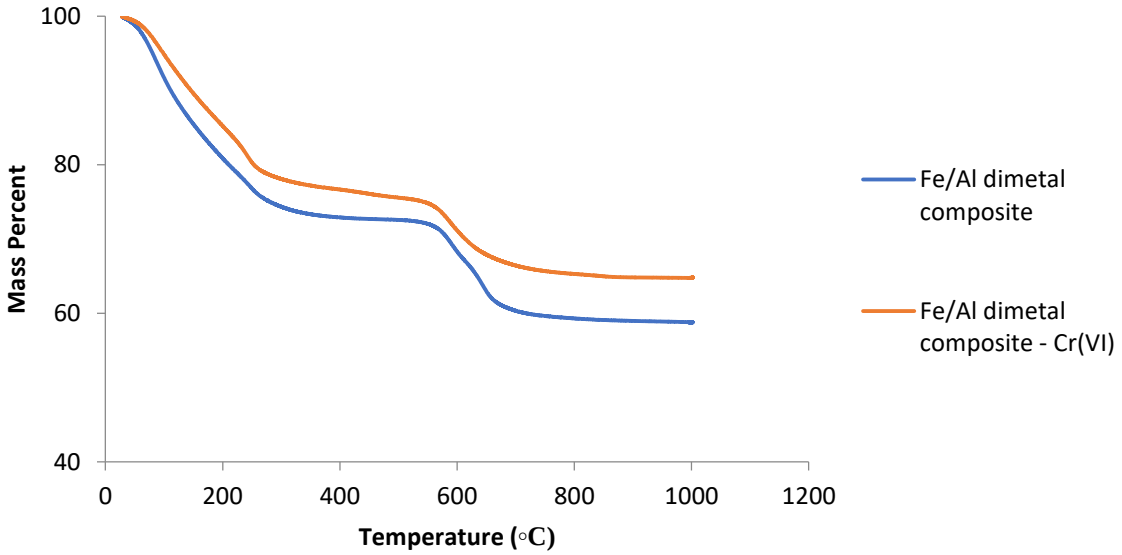

Figure 9. Thermal stability of the PDFe/Al before and after Cr(VI) adsorption.

3.2. Batch Adsorption Experiments

The effects of operational parameters on the removal of Cr(VI), as summarised in Table 1, are illustrated in Figure 10.

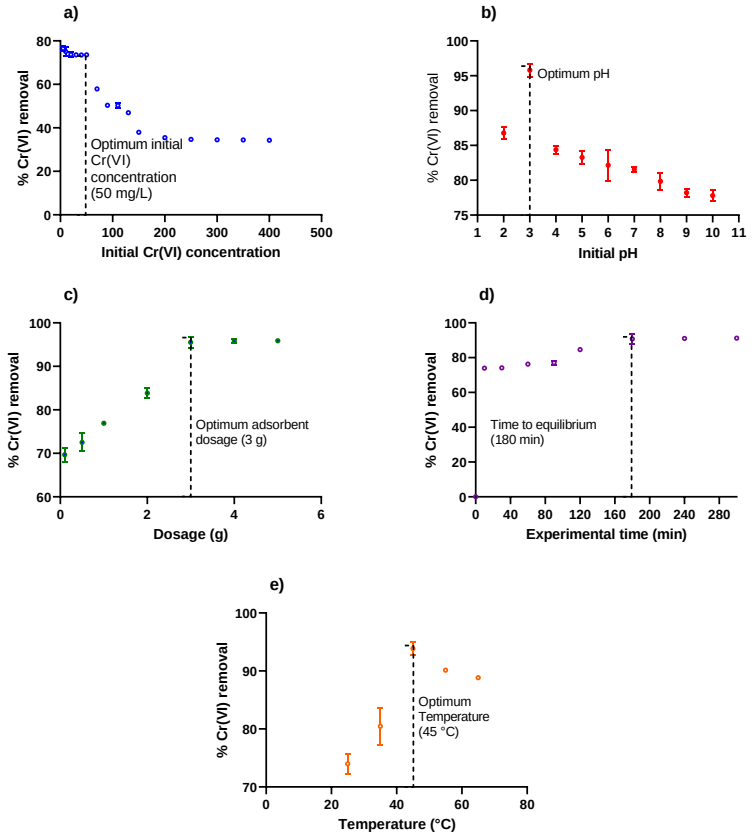

Figure 10. Effects of different operational parameters on the adsorption of Cr(VI), where (**a**) shows % Cr(VI) removal versus initial Cr(IV) concentration; (**b**) shows % Cr(VI) versus initial pH; (**c**) shows % Cr(VI) removal versus dosage; (**d**) shows % Cr(VI) removal versus agitation time; and (**e**) shows % Cr(VI) removal versus temperature.

3.2.1. Effect of Concentration

As illustrated in Figure 10a, a steep increase in the residual concentration of Cr(VI) is observed after 50 mg/L, thus indicating that the material became oversaturated with Cr(VI) oxyanions. After 50 mg/L, an increase in the residual concentration is observed, thus indicating over-saturation of the adsorbent matrices with Cr(VI) oxyanions. This indicates that the material could not adsorb Cr(IV) oxyanions of concentration >50 mg/L. Therefore, it can be concluded that 50 mg/L is the optimum concentration for Cr(VI) adsorption using PDFe/Al.

3.2.2. Effect of Initial Solution pH

As illustrated in Figure 10b, a significant amount of Cr(VI) oxyanions were removed from the aqueous system at a pH of 3. This corroborates the point of zero charge (PZC) of the adsorbent which was found to be pH_{PZC} = 3.02. Moreover, [43] also reported that the adsorption of Cr(VI) on magnetite (Fe_3O_4) decreases with an increase in pH after level 3. An optimal pH = 3 was also obtained by [44]. In addition, it was observed that the final pH in all experimental runs were between 2.07 and 2.79 indicating that in all cases, except for the run in which the initial pH was 2, a decrease in pH was observed.

3.2.3. Effect of Adsorbent Dosage

As illustrated in Figure 10c, a steep increase is observed from 0.1 to 3 g during Cr(VI) removal, after which the trend takes a gentle slope. This could indicate the depletion of available sites in the adsorbent; hence, the material could not adsorb more Cr(VI) oxyanions. This behaviour is also observed in Figure 10c, where the maximum adsorption capacity of 1 g PDFe/Al in 250 mL of 10 mg/L Cr(VI) solution was observed to be approximately 1 mg/g, hence 3g of PDFe/Al nanocomposite is optimum dosage for Cr(VI) removal. Gürü et al. 2008 [45] also reported that the highest removal of chromium was observed at 3 g using diatomite.

3.2.4. Effect of Agitation Time

As illustrated in Figure 10d, it was observed that the removal of Cr(VI) from an aqueous system increases with time. After 180 min of agitation, the graph takes a gentle slope, hence no significant removal. Most studies reported 4 h as the optimal time for removal of Cr(VI) from water [46,47]. From the results, 180 min is the optimal agitation time for Cr(VI) removal.

3.2.5. Effect of Temperature

As illustrated in Figure 10e, it was observed that the removal of Cr(VI) from an aqueous system increased with an increase in temperature, particularly between 25–35 °C. Temperatures higher than 35 °C make Cr(VI) to go back into solution. Additionally, [48] also reported that maximum removal of Cr(VI) was achieved at 40 °C. Therefore, 35 °C is an ideal temperature for maximum removal of Cr(VI) from an aqueous system

3.3. Adsorption Kinetics

Adsorption kinetics for the adsorption of Cr(VI) by PDFe/Al was studied to demonstrate the mechanisms and rates of adsorption, as shown in Table 5 and Figure 11.

Figure 11 shows different kinetic models fitted to the kinetic data for the adsorption of hexavalent chromium (Cr(VI)) onto the adsorbent. As shown in Figure 11a, a good trend was obtained from the pseudo-first order (PFO) model (R^2 = 0.945). However, there seems to be a lot of uncertainty depicted by the model the future observations in respect of Cr(VI) adsorption application, thereby making it risky to apply PFO kinetic model.

In Figure 11b, a good trend was obtained from the pseudo-second order (PSO) model, where results were obtained in the same manner as PFO. However, the PSO depends on the adsorbed amount of the adsorbate. The results obtained show a better trend than PFO (R^2 = 0.962) with great prediction of the adsorption rate of Cr(VI).

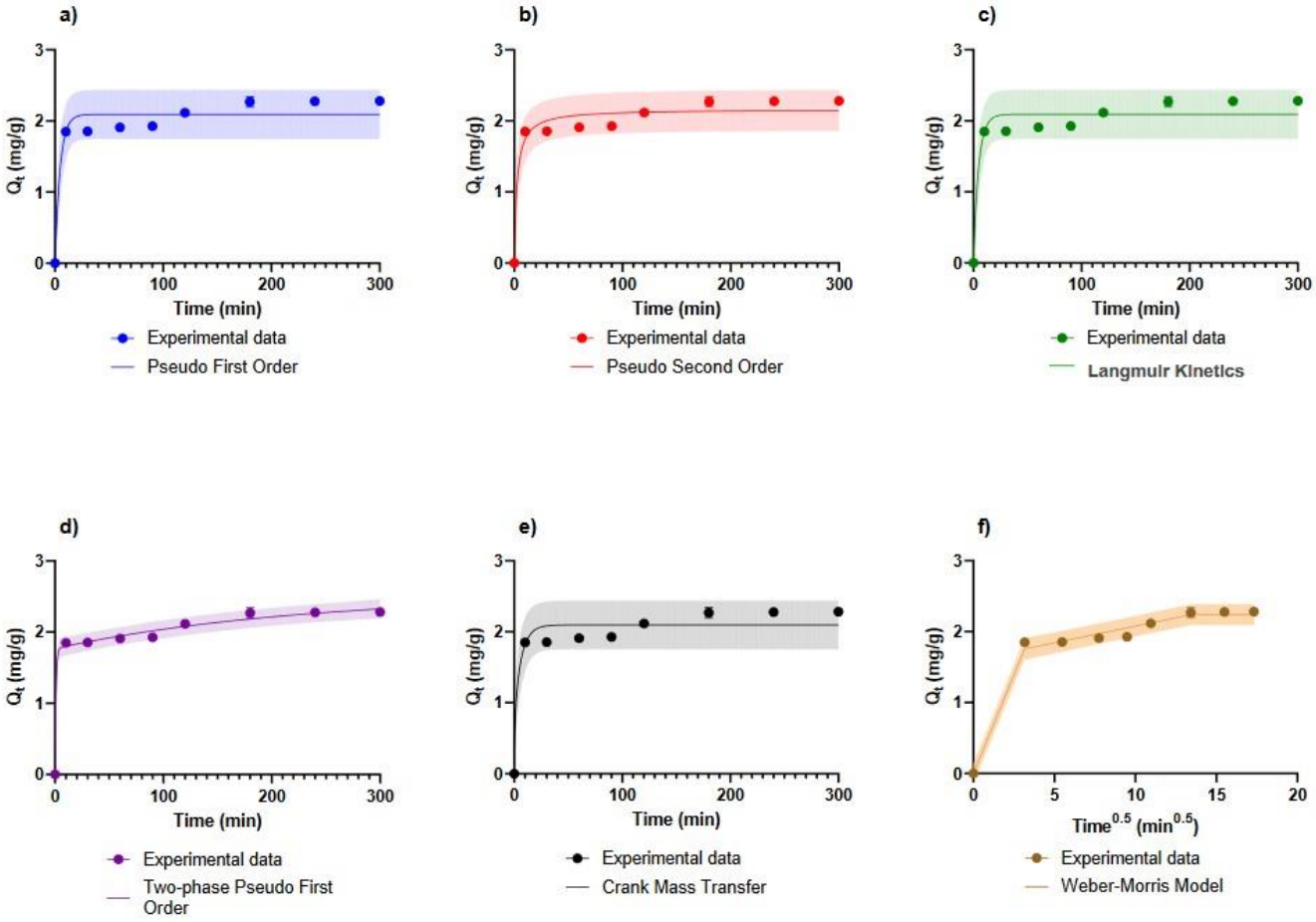

Figure 11. Different kinetic models fitted to the kinetic data for the adsorption of Cr(VI) to the adsorbent. The models were: (**a**) Pseudo First Order, (**b**) Pseudo Second Order, (**c**) Langmuir Kinetics, (**d**) Two-phase Pseudo First Order, (**e**) Crank Mass Transfer Model, (**f**) Weber-Morris Model. The shaded areas represent the 95% prediction intervals for the respective model fits. The optimised model parameters are reported in Table 5.

In Figure 11c, the Langmuir kinetics show a trend with good results (R^2 = 0.929) for the adsorption of Cr(VI); however, there is uncertainty in the diffusion and extrapolation of the model.

In Figure 11d, the two-phase pseudo-first order adsorption (TPA) model, which is based on two parallel adsorption processes: rapid and slow adsorption mechanisms, outperforms the PFO and PSO kinetic models. In comparison to previous models, the findings obtained demonstrate the best trend for Cr(VI) adsorption (R^2 = 0.993). As a result, it demonstrates how Cr(VI) is rapidly adsorbed and gradually slows down as saturation approaches.

In Figure 11e, the Crank diffusion model was investigated to determine pore diffusion since the diffusion coefficient (D_e) remains constant under the condition that the diffusion is uniform within the sphere. The results obtained show that an effective diffusion coefficient $D_e = 2.61 \times 10^{-13}$ $m^2 \cdot s^{-1}$ provides a good prediction of the Cr(VI) adsorption process. This indicates that the system is significantly limited by mass transport; the molecular diffusion coefficient of chromate is 1.4494×10^{-9} $m^2 \cdot s^{-1}$ [49] which is four orders of magnitude greater that the effective diffusivity.

Weber Morris' intra-particle diffusion model was used to study the effects of inter-particle and intra-particle diffusion on Cr(VI) adsorption in Figure 11f. The many phases of adsorption visible in the multilinear fit of the data are depicted in this model. The first phase depicts in-particle diffusion, the second phase depicts in-particle diffusion,

and the last phase depicts adsorption to the adsorbent. A good fit of the data was obtained (R^2 = 0.991) and the results showed a D_e value between D_{e1} = 7.02 × 10^{-12} $m^2 \cdot s^{-1}$ and D_{e2} = 5.11 × 10^{-13} $m^2 \cdot s^{-1}$. These results correlate well with the predicted effective diffusivity from the Crank diffusion model.

Table 5. Kinetic models for the adsorption of Cr(VI) by PDFe/Al.

Kinetic Law	Differential Form	Analytical Form	Fitted Parameters	R^2/RMSE
Pseudo first order [50]	$\frac{dQ}{dt} = k_1(Q_e - Q)$	$Q = Q_e(1 - e^{-k_1 t})$	Q_e = 2.092 mg·g^{-1} k_1 = 0.211 min^{-1}	0.945/ 0.1604 mg·g^{-1}
Pseudo second order [50]	$\frac{dQ}{dt} = k_2(Q_e - Q)^2$	$Q = \frac{(k_2 Q_e^2)t}{1+k_1 Q_e t}$	Q_e = 2.165 mg·g^{-1} k_2 = 0.188 L^2·mg^{-2}·min^{-1}	0.962/ 0.1336 mg·g^{-1}
Langmuir adsorption [51]	$\frac{dQ}{dt} = k_{ad}C(Q_{max} - Q) - \frac{k_{ad}}{K_L}Q$ $K_L = \exp\left(\frac{\Delta S^o}{R} - \frac{\Delta H^o}{RT}\right)$		k_{ad} = 0.00491 L·mg^{-1}·min^{-1} Q_{max}, ΔS^o, ΔH^o obtained from Langmuir isotherm	0.945/ 0.1603 mg·g^{-1}
Two phase adsorption [52–54]	$\frac{dQ_{slow}}{dt} = k_{fast}Q_{fast} - k_{slow}Q_{slow}$ $Q_e = Q_{fast} + Q_{slow}$	$Q = Q_{fast}\left(1 - e^{-k_{fast}t}\right)$ $+Q_{slow}\left(1 - e^{-k_{slow}t}\right)$ $Q_e = Q_{fast} + Q_{slow}$	k_{fast} = 1.11 min^{-1} Q_{fast} = 1.77 mg/g k_{slow} = 0.00444min^{-1} Q_{slow} = 0.77 mg/g	0.993/ 0.0563 mg·g^{-1}
Crank internal mass transfer model [50]	$\frac{\partial Q}{\partial t} = k_{CR}\frac{\partial}{\partial r}\left(\frac{r^2 \partial Q}{\partial r}\right)$ $k_{CR} = \frac{D_e}{r^2}$	$Q = Q_e \frac{6}{\pi^2}\sum_{n=1}^{\infty}\frac{1}{n^2}\exp(-k_{CR}n^2\pi^2 t)$ $k_{CR} = \frac{D_e}{r^2}$	D_e = 2.61× 10^{-13} m^2·s^{-1} r = 32 µm	0.946/ 0.159 mg·g^{-1}
Weber and Morris [50,55]		$Q = k_{WM}t^{\frac{1}{2}} + C$, $k_{WM} = \frac{6}{\pi^{\frac{1}{2}}}\sqrt{\frac{D_e}{r^2}}$	D_{e1} = 4.59× 10^{-13} m^2·s^{-1} r = 32 µm D_{e2} = 3.30 × 10^{-15} m^2·s^{-1} D_{e3} = 0 m^2·s^{-1}	0.991/ 0.0665 mg·g^{-1}

3.4. Adsorption Isotherms

The adsorption isotherms of Cr(VI) adsorption by PDFe/Al dimetal composite were studied on various mechanisms that determine the adsorption process. The isotherm models are summarized in Table 6 and illustrated in Figure 12.

Figure 12a depicts the Langmuir adsorption isotherm, with a maximum adsorption capacity (Q_{max}) of 6.67 mg·g^{-1}, which is acceptable for a mineral based adsorbent, especially considering that the adsorbent was recovered from authentic industrial waste AMD. To compare, Alemu et al. [56] and Panda et al. [57] tested the removal of Cr(VI) using industrially obtained basalt rock (Q_{max} = 0.079 mg·g^{-1}) and dolochar (Q_{max} = 0.904 mg·g^{-1}), respectively. In addition, the maximum adsorption capacities for comparable Fe/Al materials were in the range of 2.3–59.9 mg·g^{-1}, indicating that the current study compares well with results from the literature [26–30].

The Freundlich adsorption isotherm is shown in Figure 12b, where the intensity parameter indicates the adsorption favorability, with K_F values of K_F (298 K) = 0.8477; K_F (318 K) = 1.15; K_F (328 K) = 1.13; K_F (338 K) = 1.098. The adsorption of Cr(VI) by PDPDFe/Al from the aqueous system is highly favorable in this investigation, with n_F = 2.48.

The two-surface Langmuir adsorption isotherm is depicted in Figure 12c, which posits that the adsorbent's surface contains various surface types with varying adsorption capabilities. The results show that $Q_{max,1}$ = 1.80 mg·g^{-1} for one surface and $Q_{max,2}$ = 5.096 mg·g^{-1} for the other, for a total maximum adsorption of Q = 6.896 mg·g^{-1}.

Table 6 shows a summary of tested adsorption isotherms, fitted parameters, coefficient of determination (R^2), and root-mean-square error (RMSE) as a measure of goodness of fit for various isotherm models.

3.5. Regeneration Study

As shown in Figure 13, a regeneration study was carried out to determine the possibility of recovering and reusing PDFe/Al following Cr(VI) adsorption.

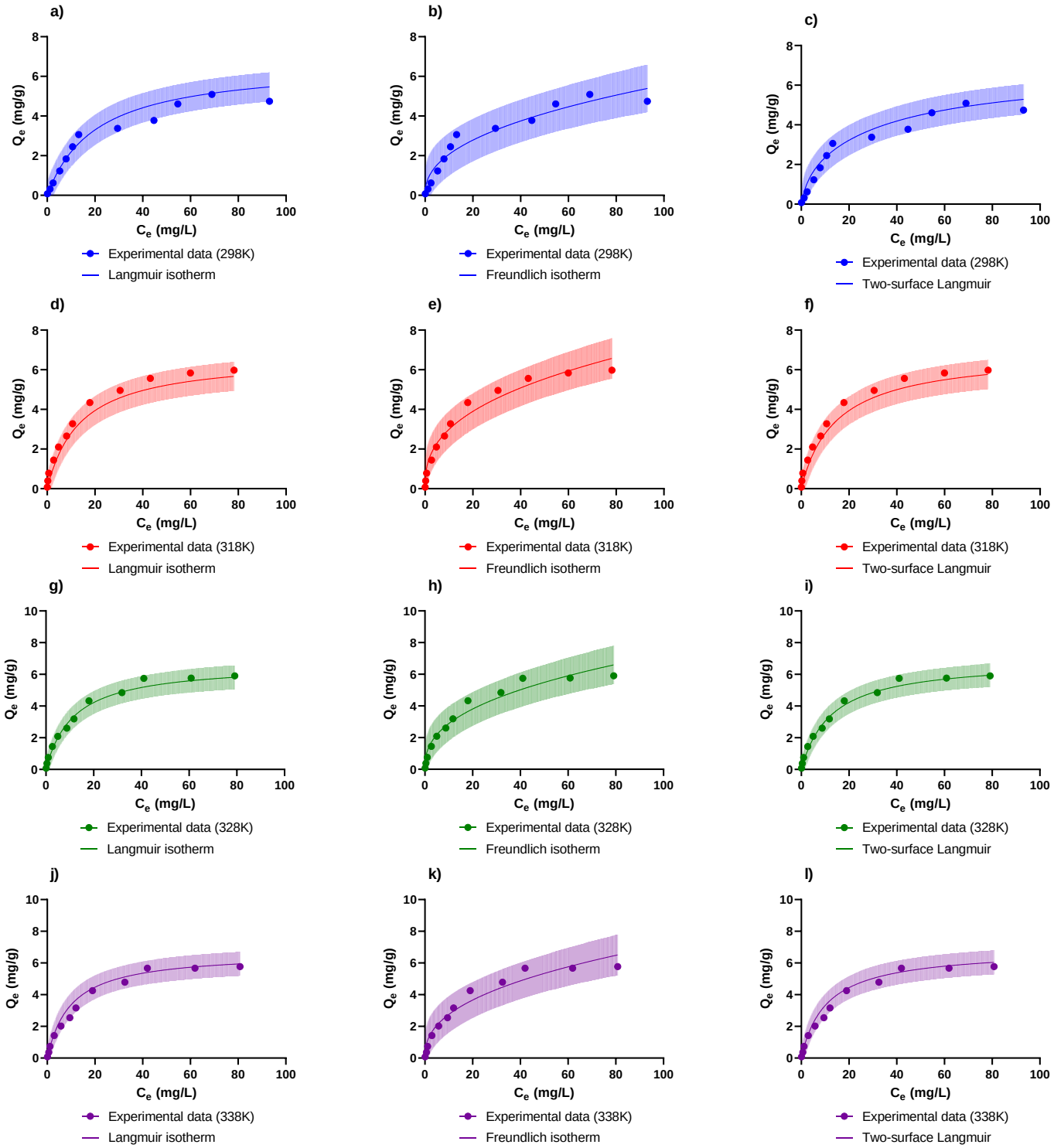

Figure 12. The non-linear fits of the isotherm models from: (**a**) Langmuir (298K), (**b**) Freundlich (298K), (**c**) Two Surface Langmuir (298K), (**d**) Langmuir (318K), (**e**) Freundlich (318K), (**f**) Two-surface Langmuir (318K), (**g**) Langmuir (328K), (**h**) Freundlich (328K), (**i**) Two-surface Langmuir (328K), (**j**) Langmuir (338K), (**k**) Freundlich (338K) and (**l**) Two-surface Langmuir (338K). The shaded areas indicate the 95% prediction intervals.

A desorption investigation was carried out to regenerate the material after Cr(VI) adsorption, as shown in Figure 13. The material had the ability to be utilized for Cr(VI) adsorption more than four times. During the first four cycles, it was observed that the

material matrices could still adsorb the oxyanions from an aqueous system. However, after four reuse cycles, it was observed that the material started losing efficacy, probably due to the loosening of the material matrices, which probably lost layers in the process of adsorption–desorption.

Table 6. Summary of tested adsorption isotherms, fitted parameters, coefficient of determination (R^2), and root-mean-square error (RMSE) as a measure of goodness of fit for various isotherm models.

Kinetic Law	Differential Form	Fitted Parameters	R^2/RMSE
Langmuir [50,58,59]	$Q_e = \frac{k_L(T)Q_{max}C_e}{1+k_L(T)C_e}$, $k_L(T) = \exp\left(\frac{\Delta S^o}{R} - \frac{\Delta H^o}{RT}\right)$	$\Delta S^o = 26.25\ J.(\text{mol·K})^{-1}$ $\Delta H^o = 15.3\ \text{kJ·mol}^{-1}$ $Q_{max} = 6.67\ \text{mg·g}^{-1}$ $0.0616 < R_L < 0.953$	0.9717/0.3412 mg·g^{-1}
Freundlich [58]	$Q_e = K_F(T)C_e^{\frac{1}{n}}$	$K_F(298\ K) = 0.8477\ \text{mg·g}^{-1}(\text{L·mg}^{-1})^{n_F^{-1}}$ $K_F(318\ K) = 1.15\ \text{mg·g}^{-1}(\text{L·mg}^{-1})^{n_F^{-1}}$ $K_F(328\ K) = 1.13\ \text{mg·g}^{-1}(\text{L·mg}^{-1})^{n_F^{-1}}$ $K_F(338\ K) = 1.098\ \text{mg·g}^{-1}(\text{L·mg}^{-1})^{n_F^{-1}}$ $n_F = 2.48$	0.959/0.410 mg·g^{-1}
Two-surface Langmuir [59]	$Q_e = \sum_{i=1}^{2} \frac{k_{L,i}(T)Q_{max,i}C_e}{1+k_{L,i}(T)C_e}$, $k_{L,i}(T) = \exp\left(\frac{\Delta S_i^o}{R} - \frac{\Delta H_i^o}{RT}\right)$	$\Delta S_1^o = -134.5\ \text{J·(mol·K)}^{-1}$ $\Delta H_1^o = -37.1\ \text{kJ·mol}^{-1}, Q_{max,1} = 1.80\ \text{mg·g}^{-1}$ $\Delta S_2^o = 76.7\ \text{J·(mol·K)}^{-1}$ $\Delta H_1^o = 32.0\ \text{kJ·mol}^{-1}, Q_{max,2} = 5.096\ \text{mg·g}^{-1}$ $0.0221 < R_{L,1} < 0.952,\ 0.0553 < R_{L,2} < 0.976$	0.975/0.320 mg·g^{-1}

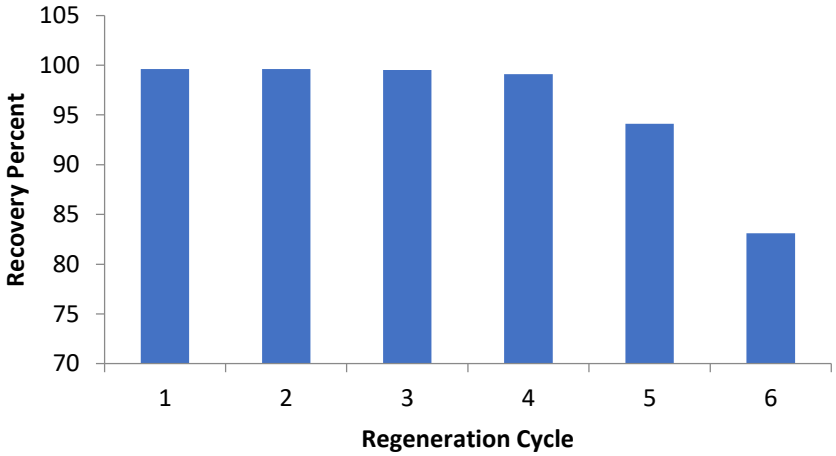

Figure 13. Recovery efficiency of PDFe/Al after Cr(VI) adsorption.

4. Discussion

4.1. Summary of Results

The results obtained in the study provide clear evidence for the potential of PDFe/Al synthesized from authentic AMD for the adsorption of Cr(VI) from aqueous solution. The surface characterization results demonstrated that the adsorption of Cr(VI) to the adsorbent involved several surface interactions with the presence of Cr(VI) and Cr(III) observed after adsorption. In addition, the adsorption of Cr(VI) resulting in adsorption induced strains within the adsorbent matrix which resulted in an increase in both the internal surface area and surface volumes. The surface analyses of the adsorbent showed the presence of Fe, O, Al, S, Cr (only after adsorption), and other minor constituents, confirming the heterogenous nature of the AMD used for the synthesis.

The batch adsorption results demonstrated that the adsorption followed a two-phase adsorption process with an initially fast process followed by a significantly slower adsorption.

The isotherm results were best described by a two-surface Langmuir kinetic model with distinct thermodynamic and saturation properties. The material further demonstrated good reusability with Cr(VI) in excess of 90% possible after five adsorption/desorption cycles.

4.2. Comparison of Fe/Al Dimetal Nanocomposite for Removal of Cr(VI) from an Aqueous System

Comparisons of rate constants, times to reach 99% of equilibrium [36], and maximum Cr(VI) adsorption capacities of different studies employing Fe- and Al-based adsorbents from the literature to the current material are made in Table 7.

Table 7. Comparison of Fe/Al dimetal nanocomposite with other Fe and Al based adsorbents in the removal of Cr(VI).

Adsorbent	Q_{max} (mg·g^{-1})	Q_e (mg·g^{-1})	k_2	$t_{2,99}$ (min) [36]	References
PDFe/Al nanocomposite	6.67	2.165	0.188 g·mg^{-2} min^{-1}	279	This study
Aluminium Oxide	78.1	72.5	6.9×10^{-4} g·mg^{-2} min^{-1}	1978	[26]
Mesoporous iron–zirconium bimetal oxide	59.88	52.46	0.02 g·mg^{-2} min^{-1}	2619	[27]
Zirconium oxide intercalated sodium montmorillonite scaffold	52.46	44.46	0.0023 g·mg^{-2} min^{-1}	2277	[28]
Hematite	2.299	0.5	0.0088 g·mg^{-2} min^{-1}	5952	[29]
Hydrochloric acid-modified kaolinite	18.15	0.34	0.089 g·mg^{-2} min^{-1}	2631	[30]
Acetic acid-modified kaolinite	10.42	0.38	0.66 g·mg^{-2} min^{-1}	513	[30]

From Table 7, it can be concluded that the synthesized Fe/Al dimetal nanocomposite demonstrated a maximum adsorption capacity comparable to other Fe and Al based adsorbents (within the same order of magnitude). In addition, it was observed that the PDFe/Al achieved equilibrium nearly an order of magnitude faster (279 min) than most of the studies (1978–5952 min), except for the acetic acid-modified kaolinite that achieved equilibrium within 513 min. These results are significant, as they demonstrate the rapidity of the adsorbent in removing the Cr(VI), a requirement for the application of an adsorption system industrially. To illustrate the point, the mesoporous iron–zirconium bimetal oxide [27] demonstrated a maximum adsorption capacity of *circa* 60 mg·g^{-1}; however, the time to 99% equilibrium took 2619 min (~44 h). This slower adsorption rate would invariably affect the residence times required for successful water treatment which negates the higher adsorption capacity displayed by the adsorbent.

In addition, the fact that the PDFe/Al dimetal nanocomposite was recovered and synthesised from authentic acid mine drainage, as opposed to synthetic chemicals, further supports the potential impact of the adsorbent as it provides an avenue for AMD valorisation through PDFe/Al synthesis and subsequent application for water treatment.

4.3. Proposed Mechanism

The results from the study indicate that the adsorption of Cr(VI) by PDFe/Al is significantly diffusion controlled with a predicted effective diffusivity of between 7.02×10^{-12} m^2·s^{-1} and 4.79×10^{-13} m^2·s^{-1} which is between 3 and 4 orders of magnitude less than the molecular diffusion coefficient of chromate (1.4494×10^{-9} m^2·s^{-1} [49]). The adsorption isotherms indicated that the surface likely consisted of at least two surfaces with distinct adsorption properties. The one surface had exothermic adsorption properties with a corresponding decrease in entropy while the other supported endothermic adsorption with an increase in entropy predicted. The decrease in entropy on the first surface likely demonstrates the increased organisation resulting from adsorption of chromium from solution, while the increased entropy on the second surface result from the displacement of protons from

the surface resulting in the observed decrease in pH [1]. It is interesting to note that the standard enthalpy and entropy values for the single surface Langmuir model were between the corresponding values from the two surface Langmuir model, indicating the single surface Langmuir model represented a net result of the two-surface model.

The results further showed that the adsorption of Cr(VI) induced significant internal strain and corresponding deformation within the support matrix which result in the formation of cracks therefore increased surface area and volume. Finally, it was observed that the adsorbed Cr(VI) was reduced to Cr(III) on the surface of the adsorbent. This likely corresponds to the oxidation of the Iron(II/III) oxide observed in the XRD profile after Cr(VI) adsorption [60]. The reduction of Cr(VI) to Cr(III) is known to have a standard Gibbs free energy of −390 kJ/mol [61] while the oxidation of Iron(II/III) oxide has a Gibbs free energy of −42 kJ/mol [61]. The resulting oxidation-reduction reaction has a standard Gibbs free energy of −450 kJ/mol and is therefore highly favourable and spontaneous.

5. Conclusions

The synthesis of polycationic di-metal iron/aluminium nanocomposite was executed through selective precipitation followed by calcination and vibratory ball milling. The material was successfully recovered and synthesised from industrial acid mine drainage and applied in the removal of hexavalent chromium (Cr(VI)) from an aqueous system. Adsorption parameters were optimized using the one-factor-at-a-time (OFAAT) approach on a batch experimental set-up. The fate of Cr(VI) in the aqueous solution, as well as the surface of the material, was determined; the results demonstrated not only the successful adsorption of Cr(VI) from solution, but also confirmed the presence and in situ reduction of Cr(VI) to Cr(III) on the surface.

Recorded optimised conditions for Cr(VI) adsorption are: 50 mg/L initial Cr(VI) concentration; 3 g of PDFe/Al; pH 3; 180 min agitation time; and temperature of 35 °C. The synthesized PDFe/Al was observed to have a Langmuir adsorption capacity of Q_{max} = 6.67 mg·g^{-1} for Cr(VI) with >95% removal.

Adsorption kinetics followed a two-phase pseudo-first-order as opposed to pseudo-first or pseudo-second-order behaviour. The adsorption process followed two-surface Langmuir adsorption model. The PDFe/Al achieved more than 90% Cr(VI) recovery after five adsorption/desorption cycles, thereby demonstrating the potential reusability.

It was proposed that a diffusion limited adsorption mechanism involving two surfaces with distinct adsorption characteristics were responsible for the adsorption. The mechanism further involved the reduction of Cr(VI) to Cr(III) while simultaneously significant internal adsorption induced strains resulted in the formation of internal cracks within the adsorbent matrix resulting in increased pore surface area and pore volume.

Comparison of the maximum adsorption capacities and time required to reach equilibrium of the PDFe/Al to literature studies demonstrated that the PDFe/Al exhibited a comparable adsorption capacity while a superior adsorption rate was measured.

This study demonstrates the industrial potential of the synthesized PDFe/Al for the simultaneous valorisation of AMD and the treatment of Cr(VI), thereby directly contributing towards sustainable mining.

Author Contributions: Conceptualization, K.L.M., V.M. and J.P.M.; methodology, K.L.M.; software, H.G.B.; validation, V.M. and H.G.B.; formal analysis, K.L.M. and H.G.B.; investigation, K.L.M.; resources, V.M., J.P.M. and H.G.B.; data curation, K.L.M., H.G.B. and V.M.; writing—original draft preparation, K.L.M., V.M. and H.G.B.; writing—review and editing, K.L.M., V.M. and H.G.B.; visualization, K.L.M. and H.G.B.; supervision, H.G.B., V.M., J.P.M.; project administration, H.G.B.; funding acquisition H.G.B. All authors have read and agreed to the published version of the manuscript.

Funding: This research was funded by the National Research Foundation (NRF) South Africa, grant number MND200517522430 and 145848. Austrian Agency for International Cooperation in Education and Research (OeAD): Africa UniNet P056.

Data Availability Statement: The data presented in this study are openly available in the University of Pretoria Research Data Repository at https://doi.org/10.25403/UPresearchdata.21342765.

Conflicts of Interest: The authors declare no conflict of interest.

References

1. Muedi, K.L.; Brink, H.G.; Masindi, V.; Maree, J.P. Effective removal of arsenate from wastewater using aluminium enriched ferric oxide-hydroxide recovered from authentic acid mine drainage. *J. Hazard. Mater.* **2021**, *414*, 125491. [CrossRef] [PubMed]
2. Muedi, K.L.; Masindi, V.; Maree, J.P.; Haneklaus, N.; Brink, H.G. Effective Adsorption of Congo Red from Aqueous Solution Using Fe/Al Di-Metal Nanostructured Composite Synthesised from Fe(III) and Al(III) Recovered from Real Acid Mine Drainage. *Nanomaterials* **2022**, *12*, 776. [CrossRef] [PubMed]
3. Baker, B.J.; Banfield, J.F. Microbial communities in acid mine drainage. *FEMS Microbiol. Ecol.* **2003**, *44*, 139–152. [CrossRef]
4. Amos, R.T.; Blowes, D.W.; Bailey, B.L.; Sego, D.C.; Smith, L.; Ritchie, A.I.M. Waste-rock hydrogeology and geochemistry. *Appl. Geochem.* **2015**, *57*, 140–156. [CrossRef]
5. Sheoran, V.; Sheoran, A.; Choudhary, R.P. Biogeochemistry of acid mine drainage formation: A review. In *Mine Drainage and Related Problems*; Nova Science Publishers Inc.: Hauppauge, NY, USA, 2011; pp. 119–154.
6. Sheoran, A.; Sheoran, V.; Choudhary, R.P. Geochemistry of acid mine drainage: A review. *Perspect. Environ. Res.* **2011**, *4*, 217–243.
7. Naidu, G.; Ryu, S.; Thiruvenkatachari, R.; Choi, Y.; Jeong, S.; Vigneswaran, S. A critical review on remediation, reuse, and resource recovery from acid mine drainage. *Environ. Pollut.* **2019**, *247*, 1110–1124. [CrossRef]
8. Cheng, H.; Hu, Y.; Luo, J.; Xu, B.; Zhao, J. Geochemical processes controlling fate and transport of arsenic in acid mine drainage (AMD) and natural systems. *J. Haz. Mat* **2009**, *165*, 13–26. [CrossRef]
9. Masindi, V.; Foteinis, S.; Chatzisymeon, E. Co-treatment of acid mine drainage and municipal wastewater effluents: Emphasis on the fate and partitioning of chemical contaminants. *J. Haz. Mat* **2022**, *421*, 126677. [CrossRef]
10. Masindi, V.; Fosso-Kankeu, E.; Mamakoa, E.; Nkambule, T.T.I.; Mamba, B.B.; Naushad, M.; Pandey, S. Emerging remediation potentiality of struvite developed from municipal wastewater for the treatment of acid mine drainage. *Environ. Res.* **2022**, *210*, 112944. [CrossRef]
11. Dhal, B.; Thatoi, H.N.; Das, N.N.; Pandey, B.D. Chemical and microbial remediation of hexavalent chromium from contaminated soil and mining/metallurgical solid waste: A review. *J. Hazard. Mater.* **2013**, *250–251*, 272–291. [CrossRef]
12. Papp, J.F. *Mineral Commodity Summaries*; U.S. Geological Survey: Reston, VA, USA, 2017.
13. Zhang, Y.K.; Qi, S.; Chen, H.H. A review of remediation of chromium contaminated soil by washing with chelants. *Adv. Mater. Res.* **2014**, *838–841*, 2625–2629. [CrossRef]
14. Sultana, M.Y.; Akratos, C.S.; Pavlou, S.; Vayenas, D.V. Chromium removal in constructed wetlands: A review. *Int. Biodeterior. Biodegrad.* **2014**, *96*, 181–190. [CrossRef]
15. Jobby, R.; Jha, P.; Yadav, A.K.; Desai, N. Biosorption and biotransformation of hexavalent chromium [Cr(VI)]: A comprehensive review. *Chemosphere* **2018**, *207*, 255–266. [CrossRef]
16. Shahid, M.; Shamshad, S.; Rafiq, M.; Khalid, S.; Bibi, I.; Niazi, N.K.; Dumat, C.; Rashid, M.I. Chromium speciation, bioavailability, uptake, toxicity and detoxification in soil-plant system: A review. *Chemosphere* **2017**, *178*, 513–533. [CrossRef] [PubMed]
17. WHO. Guidelines for drinking-water quality. In *Fourth Edition Incorporating the First Addendum*; WHO: Geneva, Switzerland, 2017.
18. Wang, Z.; Shen, Q.; Xue, J.; Guan, R.; Li, Q.; Liu, X.; Jia, H.; Wu, Y. 3D hierarchically porous NiO/NF electrode for the removal of chromium(VI) from wastewater by electrocoagulation. *Chem. Eng. J.* **2020**, *402*, 126151. [CrossRef]
19. Giagnorio, M.; Steffenino, S.; Meucci, L.; Zanetti, M.C.; Tiraferri, A. Design and performance of a nanofiltration plant for the removal of chromium aimed at the production of safe potable water. *J. Environ. Chem. Eng.* **2018**, *6*, 4467–4475. [CrossRef]
20. Melak, F.; Du Laing, G.; Ambelu, A.; Alemayehu, E. Application of freeze desalination for chromium (VI) removal from water. *Desalination* **2016**, *377*, 23–27. [CrossRef]
21. Shao, Z.; Huang, C.; Wu, Q.; Zhao, Y.; Xu, W.; Liu, Y.; Dang, J.; Hou, H. Ion exchange collaborating coordination substitution: More efficient Cr(VI) removal performance of a water-stable CuII-MOF material. *J. Hazard. Mater.* **2019**, *378*, 120719. [CrossRef]
22. Kretschmer, I.; Senn, A.M.; Meichtry, J.M.; Custo, G.; Halac, E.B.; Dillert, R.; Bahnemann, D.W.; Litter, M.I. Photocatalytic reduction of Cr(VI) on hematite nanoparticles in the presence of oxalate and citrate. *Appl. Catal. B Environ.* **2019**, *242*, 218–226. [CrossRef]
23. Kalita, E.; Baruah, J. 16—Environmental remediation. In *Colloidal Metal Oxide Nanoparticles*; Thomas, S., Tresa Sunny, A., Velayudhan, P., Eds.; Elsevier: Amsterdam, The Netherlands, 2020; pp. 525–576. [CrossRef]
24. Islam, M.A.; Angove, M.J.; Morton, D.W. Recent innovative research on chromium (VI) adsorption mechanism. *Environ. Nanotechnol. Monit. Manag.* **2019**, *12*, 100267. [CrossRef]
25. Dimos, V.; Haralambous, K.J.; Malamis, S. A review on the recent studies for chromium species adsorption on raw and modified natural minerals. *Crit. Rev. Environ. Sci. Technol.* **2012**, *42*, 1977–2016. [CrossRef]
26. Alvarez-Ayuso, E.; Garcia-Sanchez, A.; Querol, X. Adsorption of Cr(VI) from synthetic solutions and electroplating wastewaters on amorphous aluminium oxide. *J. Hazard. Mater.* **2007**, *142*, 191–198. [CrossRef] [PubMed]
27. Wang, Y.; Liu, D.; Lu, J.; Huang, J. Enhanced adsorption of hexavalent chromium from aqueous solutions on facilely synthesized mesoporous iron-zirconium bimetal oxide. *Colloids Surf. A-Physicochem. Eng. Asp.* **2015**, *481*, 133–142. [CrossRef]

28. Rathinam, K.; Atchudan, R.; Edison, T. Zirconium oxide intercalated sodium montmorillonite scaffold as an effective adsorbent for the elimination of phosphate and hexavalent chromium ions. *J. Environ. Chem. Eng.* **2021**, *9*, 106053. [CrossRef]
29. Adegoke, H.; Adekola, F. Equilibrium sorption of hexavalent chromium from aqueous solution using synthetic hematite. *Colloid J.* **2012**, *74*, 420–426. [CrossRef]
30. Dim, P.; Mustapha, L.; Termtanun, M.; Okafor, J. Adsorption of chromium (VI) and iron (III) ions onto acid-modified kaolinite: Isotherm, kinetics and thermodynamics studies. *Arab. J. Chem.* **2021**, *14*, 103064. [CrossRef]
31. Smičiklas, I.; Milonjić, S.K.; Pfendt, P.; Raičević, S. The point of zero charge and sorption of cadmium (II) and strontium (II) ions on synthetic hydroxyapatite. *Sep. Purif. Technol.* **2000**, *18*, 185–194. [CrossRef]
32. Kumari, P.; Sharma, P.; Srivastava, S.; Srivastava, M.M. Biosorption studies on shelled Moringa oleifera Lamarck seed powder: Removal and recovery of arsenic from aqueous system. *Int. J. Miner. Process.* **2006**, *78*, 131–139. [CrossRef]
33. Bordoloi, S.; Nath, S.K.; Gogoi, S.; Dutta, R.K. Arsenic and iron removal from groundwater by oxidation–coagulation at optimized pH: Laboratory and field studies. *J. Hazard. Mater.* **2013**, *260*, 618–626. [CrossRef]
34. Naiya, T.K.; Singha, B.; Das, S.K. FTIR Study for the Cr(VI) Removal from Aqueous Solution Using Rice Waste. In Proceedings of the International Conference on Chemistry and Chemical Process, Singapore, 25–28 February 2019.
35. Tang, B.; Ge, J.; Zhuo, L.; Wang, G.; Niu, J.; Shi, Z.; Dong, Y. A facile and controllable synthesis of gamma-Al_2O_3 nanostructures without a surfactant. *Eur. J. Inorg. Chem.* **2005**, *2005*, 4366–4369. [CrossRef]
36. Prabakaran, E.; Pillay, K.; Brink, H. Hydrothermal synthesis of magnetic-biochar nanocomposite derived from avocado peel and its performance as an adsorbent for the removal of methylene blue from wastewater. *Mater. Today Sustain.* **2022**, *18*, 100123. [CrossRef]
37. Hwang, S.; Umar, A.; Dar, G.; Kim, S.; RI, B. Synthesis and characterization of iron oxide nanoparticles for phenyl hydrazine sensor applications. *Sens. Lett.* **2014**, *12*, 97–101. [CrossRef]
38. Bhatt, R.; Sreedhar, B.; Padmaja, P. Chitosan supramolecularly cross linked with trimesic acid—Facile synthesis, characterization and evaluation of adsorption potential for chromium(VI). *Int. J. Biol. Macromol.* **2017**, *104*, 1254–1266. [CrossRef] [PubMed]
39. Ablouh, E.; Hanani, Z.; Eladlani, N.; Rhazi, M.; Taourirte, M. Chitosan microspheres/sodium alginate hybrid beads: An efficient green adsorbent for heavy metals removal from aqueous solutions. *Sustain. Environ. Res.* **2019**, *29*, 1–11. [CrossRef]
40. Xia, Z.; Baird, L.; Zimmerman, N.; Yeager, M. Heavy metal ion removal by thiol functionalized aluminum oxide hydroxide nanowhiskers. *Appl. Surf. Sci.* **2017**, *416*, 565–573. [CrossRef]
41. Peak, D.; Ford, R.G.; Sparks, D.L. An in situ ATR-FTIR investigation of sulfate bonding mechanisms on goethite. *J. Colloid Interface Sci.* **1999**, *218*, 289–299. [CrossRef]
42. Ou, J.; Sheu, Y.; Tsang, D.; Sun, Y.; Kao, C. Application of iron/aluminum bimetallic nanoparticle system for chromium-contaminated groundwater remediation. *Chemosphere* **2020**, *256*, 127158. [CrossRef]
43. Gallios, G.P.; Vaclavikova, M. Removal of chromium (VI) from water streams: A thermodynamic study. *Environ. Chem. Lett.* **2008**, *6*, 235–240. [CrossRef]
44. Yang, J.; Yu, M.; Chen, W. Adsorption of hexavalent chromium from aqueous solution by activated carbon prepared from longan seed: Kinetics, equilibrium and thermodynamics. *J. Ind. Eng. Chem.* **2015**, *21*, 414–422. [CrossRef]
45. Gürü, M.; Venedik, D.; Murathan, A. Removal of trivalent chromium from water using low-cost natural diatomite. *J. Hazard. Mater.* **2008**, *160*, 318–323. [CrossRef]
46. Hu, C.-Y.; Lo, S.-L.; Liou, Y.-H.; Hsu, Y.-W.; Shih, K.; Lin, C.-J. Hexavalent chromium removal from near natural water by copper–iron bimetallic particles. *Water Res.* **2010**, *44*, 3101–3108. [CrossRef] [PubMed]
47. Gaffer, A.; Al Kahlawy, A.A.; Aman, D. Magnetic zeolite-natural polymer composite for adsorption of chromium (VI). *Egypt. J. Pet.* **2017**, *26*, 995–999. [CrossRef]
48. Enniya, I.; Rghioui, L.; Jourani, A. Adsorption of hexavalent chromium in aqueous solution on activated carbon prepared from apple peels. *Sustain. Chem. Pharm.* **2018**, *7*, 9–16. [CrossRef]
49. Iadicicco, N.; Paduano, L.; Vitagliano, V. Diffusion coefficients for the system potassium chromate water at 25 degrees C. *J. Chem. Eng. Data* **1996**, *41*, 529–533. [CrossRef]
50. Largitte, L.; Pasquier, R. A review of the kinetics adsorption models and their application to the adsorption of lead by an activated carbon. *Chem. Eng. Res. Des.* **2016**, *109*, 495–504. [CrossRef]
51. Chu, K.H. Fixed bed sorption: Setting the record straight on the Bohart-Adams and Thomas models. *J. Hazard. Mater.* **2010**, *177*, 1006–1012. [CrossRef]
52. Brusseau, M.L.; Jessup, R.E.; Suresh, P.; Rao, C. Nonequilibrium Sorption of Organic Chemicals: Elucidation of Rate-Limiting Processes. *Environ. Sci. Technol.* **1991**, *25*, 134–142. [CrossRef]
53. Cornelissen, G.; VanNoort, P.; Parsons, J.; Govers, H. Temperature dependence of slow adsorption and desorption kinetics of organic compounds in sediments. *Environ. Sci. Technol.* **1997**, *31*, 454–460. [CrossRef]
54. Wang, Z.; Zhao, J.; Song, L.; Mashayekhi, H.; Chefetz, B.; Xing, B. Adsorption and desorption of phenanthrene on carbon nanotubes in simulated gastrointestinal fluids. *Environ. Sci. Technol.* **2011**, *45*, 6018–6024. [CrossRef]
55. Weber, W.J.; Morris, J.C. Kinetics of Adsorption on Carbon from Solution. *J. Sanit. Eng. Div.* **1963**, *89*, 31–60. [CrossRef]
56. Alemu, A.; Lemma, B.; Gabbiye, N.; Alula, M.; Desta, M. Removal of chromium (VI) from aqueous solution using vesicular basalt: A potential low cost wastewater treatment system. *Heliyon* **2018**, *4*, e00682. [CrossRef] [PubMed]

57. Panda, H.; Tiadi, N.; Mohanty, M.; Mohanty, C.R. Studies on adsorption behavior of an industrial waste for removal of chromium from aqueous solution. *S. Afr. J. Chem. Eng.* **2017**, *23*, 132–138. [CrossRef]
58. Girods, P.; Dufour, A.; Fierro, V.; Rogaume, Y.; Rogaume, C.; Zoulalian, A.; Celzard, A. Activated carbons prepared from wood particleboard wastes: Characterisation and phenol adsorption capacities. *J. Hazard. Mater.* **2009**, *166*, 491–501. [CrossRef] [PubMed]
59. Langmuir, I. The adsorption of gases on plane surfaces of glass, mica and platinum. *J. Am. Chem. Soc.* **1918**, *40*, 1361–1403. [CrossRef]
60. Chang, J.; Wang, H.; Zhang, J.; Xue, Q.; Chen, H. New insight into adsorption and reduction of hexavalent chromium by magnetite: Multi-step reaction mechanism and kinetic model developing. *Colloids Surf. A-Physicochem. Eng. Asp.* **2021**, *611*, 125784. [CrossRef]
61. Vansek, P. *Corrosion: Materials*; Electrochemical Series; CRC Press: London, UK, 2018; pp. 665–671.